Germanene-like defects in amorphous germanium revealed by three-dimensional visualization of high-resolution pair-distribution functions

B. Tomberli, A. Rahemtulla, E. Kim, S. Roorda, and S. Kycia

Phys. Rev. B **92**, 064204 — Published 25 August 2015

DOI: 10.1103/PhysRevB.92.064204

Germanene-like defects in amorphous germanium revealed by three dimensional visualization of high resolution pair distribution functions

B. Tomberli,[1,2] A. Rahemtulla,[1] E. Kim,[1] S. Roorda,[3] and S. Kycia[1,*]

[1]*Dept. of Physics, University of Guelph, Guelph, Ontario, Canada*
[2]*Dept. of Physics, Capilano University, North Vancouver, British Columbia, Canada*[†]
[3]*Dept. of Physics, Universite de Montreal, Montreal, Quebec, Canada*

(Dated: July 8, 2015)

The structural description of even the most basic monatomic amorphous materials are under considerable debate. In this work, an intuitive computational technique has been developed to construct 3D statistical density maps to directly visualize local atomic structure of amorphous germanium (a-Ge) enabling the interpretation of recent state-of-the-art experiments and simulations. The continuous random network (CRN) model is compared to our experimental model refined through a reverse monte carlo routine. In this refinement a-Ge has two dominant structures; a 4-fold coordinated tetrahedron and a buckled 3-fold coordinated local structure similar to silicene and germanene. These structures account for 95.7% of the total atoms in a 5:2 ratio respectively. Our method shows well defined structural ordering in the second shell of a-Ge. This novel visualization tool enables the interpretation of complex disordered materials and reveals the bimodal structures of a-Ge.

I. INTRODUCTION

The discovery and understanding of new amorphous materials drives innovation in areas such as semiconductor[1], data storage[2], energy storage, and biomedical technologies[3]. Consequently, there is currently a great deal of theoretical and experimental effort being directed towards an ever better understanding of amorphous structure[4–6]. Experimentalists have been able to capture radial distribution functions with unprecedented resolution, resolving structural details previously hidden and yet to be understood[7]. Given the lack of analytical models for amorphous structures, theorists have taken advantage of increases in computing power by incorporating first principles[6] or empirical[8] potentials in molecular dynamics[9] and monte carlo[10] approaches to make predictions of the underlying structures that exist in real samples.

In contrast to their crystalline counterparts, the interpretation of theoretical and experimentally-derived amorphous structures falls relatively short. While crystal analysis has benefited greatly from bond length and angle distributions, the broad range of bond lengths and angles for an amorphous sample[10–12] makes these metrics limiting at best. Visual techniques such as charge density maps for crystals, do not yet have an analogous counterpart tractable for the disordered nature of amorphous samples. With the vastly different structures observed in amorphous systems from metallic glasses to silica to polymers, researchers have consistently turned to amorphous silicon (a-Si) and amorphous germanium (a-Ge) as the archetypical amorphous system. Despite the many models for a-Si and a-Ge, a description for the observed undercoordination and signature features present in high resolution pair correlation functions (PCFs) is yet to be found[7,13]. Thus, an effective method is needed to properly visualize and compare differences between models.

The Continuous Random Network (CRN) model is widely applied to a-Si, a-Ge and similar covalently bonded systems[9]. The CRN model assumes local tetrahedral ordering to describe experimental PCFs. However, it is limited to 4-fold coordination, whereas experimental PCFs from high-resolution x-ray scattering measurements present undercoordination for both a-Si and a-Ge. Observed undercoordination is more pronounced in a-Ge than a-Si[14], making a-Ge a particularly interesting system to investigate.

In this work, we present a new method used to obtain density contour plots of local atomic density around a central atom. Our method preserves information about the small local variations in structure inherent in amorphous materials rather than categorizing structures according to their similarity to related crystalline structures. The rotations in our method are rigid and do not change the atomic spacings present in the original data set. The rotations are accomplished using quaternions to produce averaged three-dimensional local atomic structures which we call Local Atomic Motifs (LAMs). By visualizing the local structures from computational models using the LAM approach, we show the qualitative and quantitative structural differences between the CRN and an adjusted model arrived at by RMC refining the CRN to experimental data.

II. PREVIOUS METHODS

Recent attempts at understanding local order[4–6] have numerated the Voronoi polyhedra occurring in complex amorphous alloy structures[15] and quasicrystals[16]. In this method, the variations of the atomic positions in the first coordination shell are sorted by coordination number and geometry. The resulting geometries may be visualized to determine the structure-to-property relationship. This has been applied to systems where high coordination restricts short-range variations to a small number of local

geometries. In amorphous materials such binning operations can only be approximate due to the continuous nature of the variations in the local structure. For systems such as a-Si and a-Ge with predominantly tetrahedral local structure, the nearest neighbour atoms alone do not exclusively complete a Voronoi polyhedron. Thus, disorder beyond the first shell atoms results in many thousands of possible polyhedra. Consequently, no new insights into the structure of a-Ge and a-Si have been published using this method.

In amorphous solids, three-dimensional visualization of local order has seen comparatively little progress. The only previous work going beyond the ball-and-stick model is that of Fang *et al.*[17] who identified structural symmetries by averaging the resultant densities from a cluster alignment. This approach was one of the first of its kind and allowed bulk metallic glasses to be probed in a new way. However, in effecting the rotations and translations required to stack all the local structures on top of one another for averaging, great care must taken to preserve the interatomic distances as obtained from experiment. A cluster alignment designed to facilitate a visualization must have a strictly geometric nature. The method proposed by Fang *et al.*[17] relaxes the interatomic positions during rotation using a fictitious spring-like potential to facilitate a quasi-rigid rotation and hence may introduce more order than was present in the experimental data alone. Modifications that change the relative distances between atoms require a physical justification which is lacking in the results of Fang et al[17] and hence, their results are not quantitative. In order to advance the field a quantitative visualization method for studying amorphous structures is needed. Designing such an approach is goal of this work.

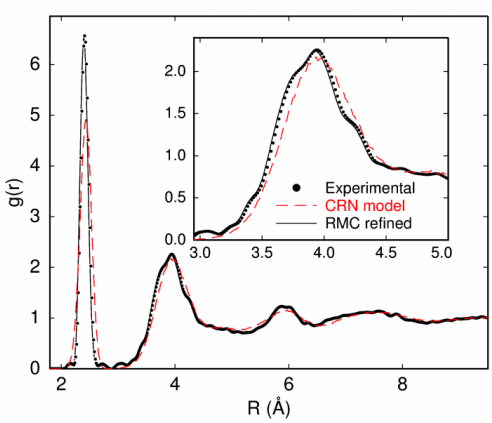

FIG. 1: Normalized pair correlation functions of a-Ge. Experimental data[14] is compared to the CRN model[18] and the RMC refined data from the CRN seed[19]. Inset highlights the second coordination shell features. The refined model fits excellently with the experimental PCF, matching all the features that do not exist in the CRN model.

III. METHODS

A. Experiment and Samples

The a-Ge sample was created by implantation of Ge ions into crystalline Ge with incident energies spanning a range of 0.5 MeV to 5 MeV. High-resolution Pair Distribution Function measurements (up to 40 Å^{-1}), were carried out at the Cornell High Energy Synchrotron Source (CHESS)[14] and the published results are used as a starting point for this work. A PCF of a-Ge, obtained from the CRN model is shown in Figure 1 along with an experimentally-obtained PCF, as measured by Roorda *et al*[14]. The CRN PCF matches qualitatively with experiment, however there is a significant disagreement between the CRN model and the experimental data in terms of peak height. This is because the first coordination peak of the experimental PCF is extremely sharp and resolution limited while the CRN peak is relatively broad. The comparison of the areas under the first peak is noteworthy because the CRN model is constrained to a coordination number of 4.00, in contrast to the experimental coordination number of 3.68 ± 0.02. The second correlation peak of the CRN model also lacks the asymmetric features present in experimental PCFs.

B. Reverse Monte Carlo

A reverse Monte Carlo (RMC) algorithm is applied to the experimentally obtained PCF to recreate the 3D atomic configuration. The resulting RMC refined PCF can be seen in Fig. 1. The program (*RMC++*[20]) used the metropolis algorithm for a 100,000 atom configuration with periodic boundary conditions. In contrast to the works of Cai *et al.*[12] and Biswas *et al.*[10], no additional constraints were applied to the RMC simulation. The initial configuration was created by Barkema and Mousseau[18] based on a CRN method called the Wooten-Winer-Weaire model[9]. The CRN model was originally created for a-Si with spatial dimensions scaled to coincide with a-Ge. The RMC modelling matched the experimental data after 10^7 steps and the resulting atomic configuration is included as a supplemental data set. The first coordination peak has been properly refined through RMC and the asymmetry in the second peak shown in the inset has also been captured in the refined model.

C. Traditional Analysis

The RMC refinement is indeed successful at matching the experimental PCF, which can be seen in figure 1. This makes the 100,000 atom model the only model that accurately matches experimental data to the accuracy provided here. However, without a potential, it is reasonably possible that the moves could create a system that is entirely unreasonable. A traditional check, which also gives an insight as to how undercoordination manifested in this model is to look at the coordination number distribution as classical analysis is performed. This is shown in Table 1.

TABLE I: Number of clusters obtained for a sample coordinate set from RMC++

coordination state	amount	error
0	5	2
1	169	13
2	2870	54
3	27453	166
4	68235	261
5	1244	35
6	24	5

To investigate undercoordination, the coordination state of each of the 100,000 clusters comprising the LAM obtained from the refined coordinate set was used to generate a first shell coordination number. Due to stochastic variations inherent in the RMC process, a single configuration should not be used to obtain an average coordination number. Thus, ten configurations (and resulting PCFs) were sampled at intervals of 100,000 RMC steps. The average was used to obtain the best estimate of the coordination number and the standard deviation of these ten samples was used to estimate the error shown in Table 1. This standard deviation is indicative of the variation the RMC algorithm can produce from a single initial seed. Since a major goal of this work is to determine the degree of change required for a CRN seed to conform to the experimental PCF, other seeds were not employed and hence the variation resulting from different seeds is not known. The final coordination number, resulting from block averaging[21] over all ten sets of coordinates, is 3.674 $\pm$ 0.001. This number checks very well with the value of 3.672 $\pm$ 0.001 (all error bars are 1 σ) obtained by integration of the area under the first peak of the experimental PCF in figure 1. The 3-fold coordinated atoms, which are the dominant form of undercoordination, represent about 27.5 % of the total LAMs. Table 1 also shows that the refined model has 4-fold coordinated structure for 68.2 % of its atoms, whereas the CRN model always has all four atoms positioned about 2.4 Å from atom zero.

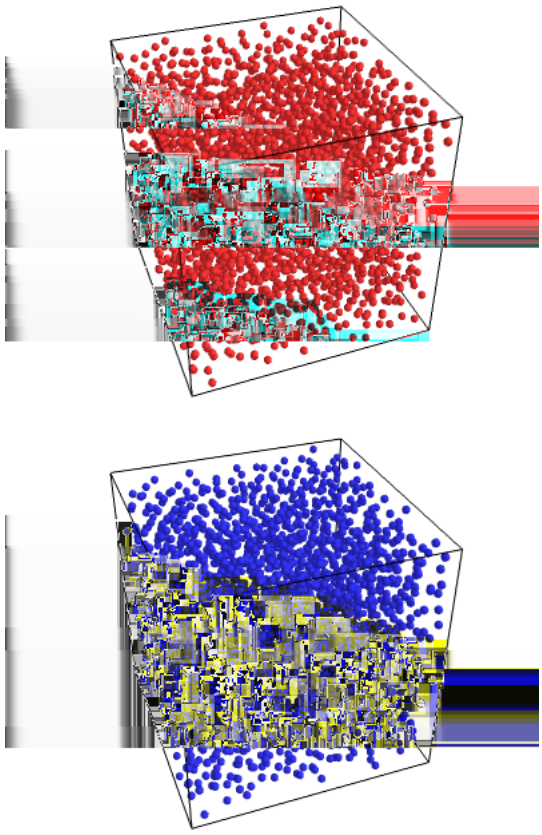

FIG. 2: Sub-coordinate set of the CRN model (top) and the refined model (bottom). Approximately 25% of the coordinate set is being displayed. RMC created a fairly uniform distribution showing no long range inhomogeneity such as cracks or voids. Due to the large numbers it is difficult to find structural differences between the two models.

Multi-atom correlation could traditionally only be understood through direct observations of the bulk model. Figure 2 depict a subset of the coordinate sets for both CRN (red) and the model refined through RMC (blue). Despite the vast differences in structure evident by the changes to the PCF (figure 1) and the coordination number distribution (table 1), there is simply too much information to process any structural details. With so many atoms, it is nearly impossible to detect if the CRN model even contains local tetrahedral ordering. Issues such as these drives analysis to statistical averaging at the expense of multi-atom correlations.

Averaging the bond angles is a common analysis tool to gauge what type of geometrical ordering could exist in the absence of a visualization technique. This analysis is shown in figure 3. The use of a large 100,000 atom CRN model produces a much smoother bond angle distribution function than what was presented earlier by Biswas *et al.*[10]. Through comparisons of large models, it is clear that there are differences in the bond angle

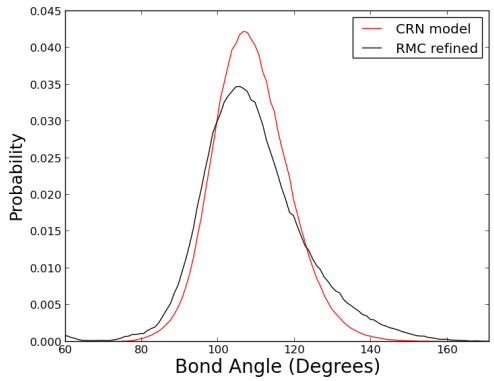

FIG. 3: Normalized bond angle distribution for the CRN model (red) and the refined model (black). The CRN model is very symmetric while the refined model is broader and asymmetric with no clear underlying cause.

distribution. The refined model depicts a broader and an asymmetric distribution. It may be possible that the asymmetries are due to the bimodal coordination number distribution. Any substantial conclusions cannot be derived solely from these types of analysis as multi-atom correlations are averaged out.

IV. LOCAL ATOMIC MOTIF METHOD

The LAM methods use of rigid rotations creates a 3D visualization that is a true representation of the bulk model, and thus allows quantitative information to be extracted as demonstrated in this work. Consequently, the bond angle distributions, bond distance distributions, PCF and even coordination number are conserved within our visualization. It is for these reasons that our method is a conceptual advancement that allows visualizations to serve a useful purpose in solving structure problems.

A. Initial LAM Orientation

The atomic structures in the CRN and refined model can be compared by translating each atom and its local arrangement to the origin and applying multiple geometric rotations to each cluster such that they are all oriented consistently using the following procedure, implemented in Python. First, an atom is chosen from the bulk structure and is labelled as atom 0. Then a fixed number of its nearest neighbours (chosen here to be 16) are found, sorted by proximity from atom 0 and labelled with numbers (1-16). This produces a cluster of 17 atoms in total, which comprise the complete first and second shells for a 4-fold coordinated crystalline system. This cluster is then translated to constrain atom 0 to the origin. The cluster is then rotated about the polar angle to bring atom 1 to the z-axis. An azimuthal rotation, about the z-axis, is then applied to the cluster, placing atom 2 on the x-z plane. These are standard rotations implemented using quaternions. This procedure is repeated for every atom in the model until all N clusters for an N atom model are superimposed on top of each other. The resulting scatter plot of atom positions is what we call the LAM and can be presented as a 3D contour plot using open-source software[22]. Figure 4 shows the resulting LAMs for the CRN model and the refined model. For the first shell of atoms, the expected simple tetrahedral structure is obtained implying 4-fold coordinated clusters dominate both LAMs. This is because 100% of the CRN atoms and 68% (see Table 1) of the refined atoms are 4-fold coordinated. In the case of 4-fold coordination: the central and upper high-density spheres correspond to atoms 0 and 1 (z-axis), respectively. The three lower clouds of intermediate density within the first shell correspond to atoms 2 (x-z plane), 3 and 4, which complete the expected tetrahedral structure. Atoms 1 and 2 uniquely occupy two corners of the tetrahedron while due to chirality from the imposed labelling, atoms 3 and 4 occupy either of the two remaining tetrahedron corner positions. This leads to the appearance of the double occupancy as shown in figure 4.

Though this method successfully creates a first look at the structure of a-Ge, it is not yet generalizable to other, non-tetrahedral systems. In the case of structures like the icosahedron, after atom 1 is rotated to the z-axis, there are three different types of atoms that could be atom 2; the upper plane, the lower plane or on the negative z-axis. The latter case is especially unfortunate as the azimuthal rotations will not serve a purpose. The following modification was created to allow this method to apply to all possible structures: a list of atoms that lie within the nearest neighbour distance is found. The first atom will then be chosen as atom 1, as usual. Of the remaining atoms, the atom with the smallest n-0-1 angle (where n is the remaining nearest neighbour atoms,) will be fixed to the x-z plane ($\phi = 0$). The resulting LAM would be effectively identical, with the only difference being a change in atom labelling.

By using 17 atom clusters in these LAMs, atoms beyond the first coordination shell are also depicted. The four diffuse ring structures at farther distances from the origin atom correspond to atoms of the second shell. Three lobes are visible in each of the four second-shell ring structures. These correspond to higher-density regions for the twelve second shell atoms. Roorda *et al.* claimed that a non-uniform dihedral angle distribution exists in a-Ge[14], but were unable to prove. The LAMs reveal strong evidence supporting this fact (Figure 4) as it is clearly seen that each second shell ring is composed of three overlapping lobes as opposed to a simple torus. The centroids of the lobes are at the approximate locations for the second shell atoms in crystalline germanium, indicating that the crystalline positions are preferred but other rotations about the 0-1 axis are allowed. The LAMs thus provide a previously unseen view of the three-dimensional

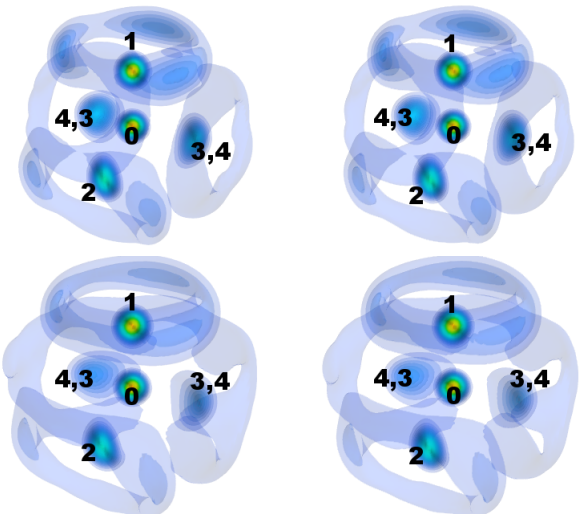

FIG. 4: Gaussian-smoothed 3D atomic density contour plot of the 17 atom LAMs for the CRN model (top) and the refined model (bottom). Each LAM is presented as a cross-eyed stereogram for 3D visualization. Warmer colours correspond to higher densities. Animated rotations of each contour plot are shown in supplemental figures 1 and 2 respectively.

local structure in a-Ge. The CRN LAM shows better defined lobes in the uppermost ring compared to the refined LAM, suggesting that the CRN model may present more ordering in this part of the second shell than is observed experimentally.

The refined LAMs appear qualitatively similar to those based on the CRN model configuration as shown in Figure 4. However, it is known that the experimental PCF yields an average coordination of 3.68 ± 0.02 for a-Ge, so it is expected that a deeper analysis of the refined LAMs will show evidence of undercoordinated Ge atoms[14]. To investigate this, we focus attention on atom 4 for a-Ge, the fourth-closest atom to atom 0. The PCFs in Figure 1 show a minimum at 2.7 Å. Clearly, this minimum corresponds to the boundary between the first and second coordination shells. In a fully coordinated Ge atom, atom 4 should be within 2.7 Å, whereas atom 4 should be farther away for an undercoordinated Ge atom.

B. Fixed Plane Orientation LAM

In order to highlight the difference in local order between fully coordinated and undercoordinated atoms, it is necessary to construct the refined LAMs for a-Ge using a different *fixed-plane orientation* method. A new method is necessary since the location of atom 4, the fourth nearest atom determines whether the cluster is 3-fold or 4-fold coordinated. In the initial LAM orientation, atom 4 existed in two possible locations, making it impossible to isolate structural effects of atom 4. While the initial LAM orientation could be modified to place atom 4 on the z-axis, it would be unwise to constrain a cluster using an unconstrained atom. Rather, we instead perform a cluster alignment based on the plane created by atoms 1-3.

Here, atom 0 of the 17 atom cluster is translated to the origin exactly as before. Then a plane is defined which contains atoms 1, 2 and 3 (123 plane). The normal of this plane (which, in crystalline Ge, would be collinear with the position vector of atom 4) is locked to the z-axis by a polar rotation of the cluster about the origin (atom 0). Then an azimuthal rotation about the z-axis places atom 1 on the x-z plane. Finally, the clusters are sorted into two groups: In one group, the clusters are fully coordinated and thus contain atoms 1-4 within 2.7 Å of atom 0. In the other group, the clusters are undercoordinated (3-fold coordinated) and atoms 1-3 are within 2.7 Å while atom 4 is at a greater distance. As before, LAMs are expressed by density contours of the resulting scatter plots. The LAMs produced by this modified procedure enable a comparison of the local arrangement around the 3-fold and 4-fold coordinated atoms. Analysis of these LAMs reveals that atom 4 in the undercoordinated LAM (top of Figure 3) is at a distance of 3.43 ± 0.02 Å from the origin. This places atom 4 within the second coordination shell of the PCF. The atom appears as a diffuse cloud directly above atom 0 losing the tetrahedral symmetry present in the fully coordinated LAM. The presence of atom 4 in this region increases the disorder in the second shell. The well defined second shell ring present in the 4-fold coordinated LAM (bottom of Figure 5) is now perturbed by 3-fold coordination (top of figure 5).

Also apparent in figure 5 is the lower position of atom 0 relative to the 123 plane for the 3-fold coordinated LAM. An analysis of the atom 0 to 123 plane distance (d) for undercoordinated LAMs yields $d = 0.45 \pm 0.02$ Å, block averaged over 10 coordinate sets. For the 4-fold coordinated LAM, the same analysis yields $d = 0.76 \pm 0.01$ Å in contrast to $d = 0.844$ Å for the CRN LAM and $d = 0.798$ Å for perfectly crystalline Ge. The LAMs thus provide clear evidence for a bimodal local structure with 3-fold coordinated atoms in about a 2:5 ratio with 4-fold coordinated atoms, with structures that both differ from the continuous random network model.

The perturbation from ideal diamond crystal structure caused by ion implantation creates a significant production of undercoordinated local structures consistent with those of 3-fold coordinated silicene and germanene[23]. The undercoordinated LAM from a-Ge has a lower d than its germanene counterpart, where germanene has $d = 0.69$ Å[24]. However, the breaking of the 0-4 bond does not lead to a planar graphene-like structure, with atom 0 in plane with atoms 1,2 and 3. Multiple checks were conducted and the buckled structure of the 3-fold coordinated LAM created through RMC refinement only occurred when refined to the experimental PCF and not when refining to the PCF of the CRN model. The resulting combination of the 3-fold and 4-fold coordinated

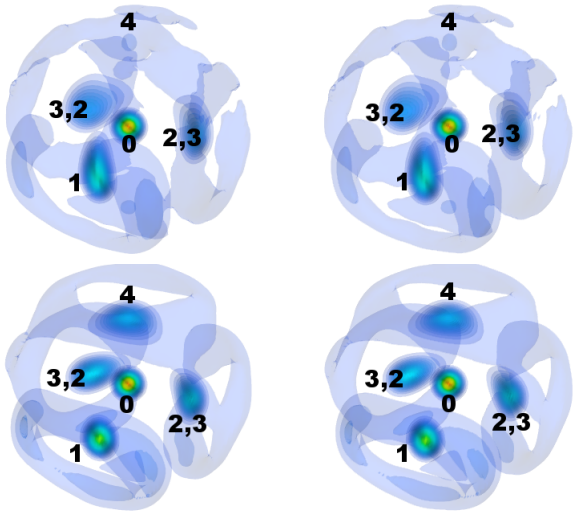

FIG. 5: Gaussian-smoothed 3D atomic density contour plot of 17 atom LAMs for the refined model. The top LAM (top) showing only 3-fold coordinated clusters where atom 4's distance from the origin is greater than 2.7 Å and the bottom LAM (bottom) showing only 4-fold coordinated clusters where atom 4's distance from the origin is within 2.7 Å. Both images are presented as cross-eyed stereograms. Animated rotations of each contour plot are shown in supplemental figures 3 and 4 respectively.

motifs introduces a new candidate structure for amorphous germanium that accounts for undercoordination.

V. CONCLUSIONS

The implementation of LAMs from atomic coordinates of a bulk model provide new insight into the local atomic structure in amorphous materials to explain previously puzzling undercoordination effects. The results imply that any theoretical model of a-Ge must include the possibility of 3-fold coordinated local motifs with structures distinctively different from the 4-fold coordinated tetrahedron. We show that the undercoordinated local structure of a-Ge are similar to germanene with the structure consistently being buckled as opposed to a planar graphene lattice. The atom 0 to 123 plane distance of undercoordinated a-Ge atoms are shorter by 0.31 ± 0.02 Å in comparison to the the 4-fold coordinated atoms. Also, strong evidence of ordering in the second shell is clearly seen. Decades ago, statistical analysis of Voronoi polyhedra enabled scientists and readers to understand models for periodic structures. The success of this approach caused an expansion of the field beyond simple alloys that continues to the present day. However, for many amorphous materials, the low nearest neighbour coordination makes interpreting Voronoi polyhedra difficult. This has hindered progress in the field. The LAM method can capture the essence of subtle differences between competing models, going beyond base geometries. This method serves as a powerful analytical tool, which will help make analogous advances in the field of amorphous structure determination. This visualization approach can be widely applied to unlock the structural solutions of other systems; from long range disorder in periodic structures to local order in amorphous and liquid structures.

* Email Address: skycia@uoguelph.ca
† Email Address: brunotomberli@capilanou.ca

[1] A. C. Wright and M. F. Thorpe, physica status solidi (b) **250**, 931 (2013), ISSN 1521-3951, http://dx.doi.org/10.1002/pssb.201248500.
[2] L. Nikolova, T. LaGrange, B. Reed, M. Stern, N. Browning, G. Campbell, J.-C. Kieffer, B. Siwick, and F. Rosei, Applied Physics Letters **97**, 203102 (2010).
[3] W. H. Wang, Advanced Materials **21**, 4524 (2009), ISSN 1521-4095, http://dx.doi.org/10.1002/adma.200901053.
[4] H. Sheng, W. Luo, F. Alamgir, J. Bai, and E. Ma, Nature **439**, 419 (2006).
[5] T. Fukunaga, K. Itoh, T. Otomo, K. Mori, M. Sugiyama, H. Kato, M. Hasegawa, A. Hirata, H. Y., and A. Hannon, Materials Transactions **48**, 1698 (2007).
[6] P. Ganesh and M. Widom, Physical Review B **77**, 014205 (2008).
[7] K. Laaziri, S. Kycia, S. Roorda, M. Chicoine, J. Robertson, J. Wang, and S. Moss, Phys. Rev. Lett. **82**, 3460 (Apr 1999), http://link.aps.org/doi/10.1103/PhysRevLett.82.3460.
[8] P. M. Voyles, N. Zotov, S. M. Nakhmanson, D. A. Drabold, J. M. Gibson, M. M. J. Treacy, and P. Keblinski, Journal of Applied Physics **90**, 4437 (2001), http://scitation.aip.org/content/aip/journal/jap/90/9/10.1063/1.1407319.
[9] F. Wooten, K. Winer, and D. Weaire, Physical Review Letters **54**, 1392 (1985).
[10] P. Biswas, R. Atta-Fynn, and D. A. Drabold, Physical Review B **69**, 195207 (May 2004).
[11] D. Polk, Journal of Non-Crystalline Solids **5**, 365 (1971).
[12] B. Cai, A. L. Goodwin, and D. A. Drabold, Modelling and Simulation in Materials Science and Engineering **19**, 035010 (Apr. 2011).

[13] R. Temkin, W. Paul, and G. A. N. Connell, Advances in Physics **22**, 581 (1973), http://dx.doi.org/10.1080/00018737300101349, http://dx.doi.org/10.1080/00018737300101349.

[14] S. Roorda, C. Martin, M. Droui, M. Chicoine, a. Kazimirov, and S. Kycia, Physical Review Letters **108**, 255501 (Jun. 2012).

[15] F. Frank and J. Kasper, Acta Crystallographica **11**, 184 (1958).

[16] W. Brostow, M. Chybicki, R. Laskowski, and J. Rybicki, Physical Review B **57**, 113448 (1998).

[17] X. W. Fang, C. Z. Wang, Y. X. Yao, Z. J. Ding, and K. M. Ho, Phys. Rev. B **82**, 184204 (Nov 2010), http://link.aps.org/doi/10.1103/PhysRevB.82.184204.

[18] G. T. Barkema and N. Mousseau, Phys. Rev. B **62**, 4985 (Aug 2000), http://link.aps.org/doi/10.1103/PhysRevB.62.4985.

[19] O. Gereben and L. Pusztai, Phys. Rev. B **50**, 14136 (Nov 1994), http://link.aps.org/doi/10.1103/PhysRevB.50.14136.

[20] O. Gereben, P. Jovari, L. Temleitner, and L. Pusztai, Journal of Optoelectronics and Advanced Materials **9**, 3021 (2007).

[21] H. Flyvbjerg and H. G. Petersen, The Journal of Chemical Physics **91**, 461 (1989), http://scitation.aip.org/content/aip/journal/jcp/91/1/10.1063/1.457480.

[22] Enthought, "Mayavi 3d visualization software: used to generate density contour plot of cluster data," http://code.enthought.com/projects/mayavi/ (Aug. 2013).

[23] A. OHare, F. V. Kusmartsev, and K. I. Kugel, Nano Letters **12**, 1045 (2012), http://pubs.acs.org/doi/pdf/10.1021/nl204283q, http://pubs.acs.org/doi/abs/10.1021/nl204283q.

[24] F. Bechstedt, L. Matthes, P. Gori, and O. Pulci, Applied Physics Letters **100**, 261906 (2012).